Construction and Building Materials 440 (2024) 137351

Contents lists available at ScienceDirect

Construction and Building Materials

journal homepage: www.elsevier.com/locate/conbuildmat

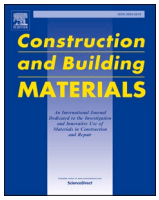

Recycling thermally detoxified asbestos-cement in stone-wool: An end-less-life material!

Giancarlo Capitani [a,*], Fabrizio Vergani [a], Roberto Conconi [a], Primož Mrvar [b], David Bombač [b], Lidija Slemenik Perše [c], Alen Oseli [c], Benjamin Bizjan [d]

[a] University of Milano Bicocca, School of Sciences, Department of Earth & Environmental Sciences, Piazza della Scienza 4, Milan 20126, Italy
[b] University of Ljubljana, Faculty of Natural Sciences, Department of Materials and Metallurgy, Lepi Pot 11, Ljubljana 1000, Slovenia
[c] University of Ljubljana, Faculty of Mechanical Engineering, Laboratory for Experimental Mechanics, Aškerčeva 6, Ljubljana 1000, Slovenia
[d] University of Ljubljana, Faculty of Mechanical Engineering, Laboratory for Water and Turbine Machines, Aškerčeva 6, Ljubljana 1000, Slovenia

ARTICLE INFO

Keywords:
Stone-wool
Asbestos-cement
Thermal detoxification
Recycling
Circular economy

ABSTRACT

Deactivated (detoxified) asbestos-cement (DAC), i.e. asbestos-cement slates thermally treated at 1100 °C in order to convert the harmful asbestos fibers into non harmful mineral phases, has been successfully mixed with 74.6 wt % quartz sand and up to 63.2 wt% basalt sand, to produce stone wool with mechanical properties and composition competitive with commercial stone wool. The sample with 50 % DAC and 50 % basalt provided the best comparison with commercial stone wool in terms of *liquidus* temperature (lower than for the other mixtures) and Young's modulus (higher). Through further composition optimization and utilization of multiple components, we estimate that future batches could utilize 70–75 % of DAC. These promising results and expectations highlight a feasible reuse of DAC as secondary raw material for stone wool production and a possible route to the elimination of a toxic waste from the environment and the preservation of primary raw materials.

1. Introduction

Asbestos is a term applied to six naturally occurring fibrous silicate minerals belonging to the phyllosilicate and amphibole mineral groups (Directive 2003/18/EC). To the former belongs chrysotile serpentine (ideally $Mg_3Si_2O_5(OH)_4$), commercially known as *white asbestos* and which accounts for 95 % of all the asbestos used in the 20th century. To the latter group belong five amphibole species, the most commercially successful forms of which were amosite ($Fe_7Si_8O_{22}(OH)_2$), also known as *brown asbestos*, and crocidolite ($Na_2Fe_3Fe_2^{3+}Si_8O_{22}(OH)_2$) or *blue asbestos*. Because of featuring notable properties such as mechanical strength, chemical resistance, and thermal insulation, asbestos has been considered a promising and strategic resource for economic growth and prosperity in the last century and extensively mined and used in various industrial sectors. Asbestos-containing materials (ACM) have been used in floor and roof tiles, surfacing materials, thermal insulation around pipes and boilers, wallboards, chimneys, water reservoirs, and many other applications [1].

However, since the early 1970s, epidemiological studies have revealed the harmful effects of asbestos e.g. [2–4] and asbestos exposure has been conclusively linked to the development of malignant mesothelioma e.g. [5–7]. Italy was among the firsts countries to ban the extraction, production, and use of asbestos in 1992. In 2005, European Union countries also prohibited the marketing and use of products containing asbestos [8]. Nevertheless, ACM are still abundant in many buildings and represent a hazard for human health. For instance, during the period 1976–1980, Italy produced around 100,000 tons per year of ACM [9] most of which are still in place. Worldwide, some 200 million tons of asbestos have been mined and used in products since 1900 [10].

In order to reduce the risk of exposure to asbestos, ACM can be managed *in situ* through sealing techniques (e.g., roof encapsulation and confinement) or by removing and landfilling it as asbestos containing waste (ACW). However, the long-term efficacy of these approaches faces some challenges. ACM that are still in place as well as ACW sites require ongoing monitoring and maintenance and are subjected to natural and extreme climate events, like sea-level rise, flooding, and earthquakes [11–14] and even terrorist attacks. In view of the limits of current strategies adopted by law to mitigate the asbestos problem, smarter solutions are required. An asbestos detoxification treatment coupled with a clear recycling route has been recommended by the European

* Corresponding author.
E-mail address: giancarlo.capitani@unimib.it (G. Capitani).

https://doi.org/10.1016/j.conbuildmat.2024.137351
Received 19 March 2024; Received in revised form 1 July 2024; Accepted 3 July 2024
Available online 19 July 2024

Parliament with the resolution of 14 March 2013 on "*Asbestos related occupational health threats and prospects for abolishing all existing asbestos* (2012/2065(INI))". Valuable revisions on the state of the art on asbestos detoxification methods are given by Spasiano and Pirozzi [15] and Paolini et al. [16].

In the present work, we thermally treated at 1100 °C in oxidizing conditions common asbestos-cement slates like Eternity ® (i.e. the main ACM nowadays still present as roofing in many public and private buildings) obtaining the decomposition of all the asbestos minerals into harmless minerals (details in Vergani et al. [17]). Then, we successfully reused the powdered product of the deactivated (detoxified) asbestos-cement (DAC) in the production of stone wool.

Stone wool is one of the most commonly used types of fibrous materials in construction industry after the asbestos ban. It is composed of fine and mutually intertwined fibers produced by spinning and blowing molten rocks at high speed. Stone wool sheets are characterized by low density and high porosity, resulting in excellent sound absorption, thermal insulation and fire resistance properties. The properties of mineral fibers depend on several design and operating parameters, as well as on the chemical composition of the melt [18]. In turn, mineral wool from demolition waste can be recycled several times in a variety of applications [19] giving rise to end-less-life material!

2. Experimental

2.1. Raw materials and stone wool recipes

Batches of deactivated asbestos-cement slates were separately mixed with basalt or quartz to accost a target normalized chemical composition of 45 % SiO_2, 20 % (Al_2O_3+ Fe_2O_3), 30 % CaO and 5 % MgO, which was selected by considering average stone wool compositions from several manufacturers. Such a composition was expected to yield fibers with mechanical and biosolubility properties similar to industrial stone wool fibers.

Deactivation of asbestos was obtained by thermally treating asbestos-cement slates (Eternit ®) in air at 1100 °C. The slates, still self-sustaining after the thermal treatment, were then powdered in a ball mill for 10 minutes. The complete disappearance of asbestos was then ascertained with a variety of analytical techniques, as well as the determination of the chemical, physical and mineralogical characteristics of the DAC, as detailed in Vergani et al. [17] Basically, the chemical composition of the DAC is dominated by CaO (~47 %), SiO_2 (~44 %), MgO (~8 %) and Al_2O_3 (~4 %) and the phase composition by glass (40 %) and some cement phases (åkermanite, bredigite and merwinite in almost similar proportions). The quartz sand is almost pure SiO_2 (~99 %), and the basalt contains SiO_2 (~40 %), Fe_2O_3 (~16 %), Al_2O_3 (~14 %), CaO (~10 %), MgO (~9 %), Na_2O (~4 %), TiO_2 (~3 %) and K_2O (~1 %) as major components (see ahead).

The procedure for designing melting batches with the target compositions is schematically illustrated in Fig. 1. Note that although mineral fibers typically contain significant amounts of other oxide components, a four-component SiO_2-(Al_2O_3+Fe_2O_3)-CaO composition normalized to the sum of 100 % was assumed in Fig. 1 to simplify the composition design process. To attain the desired target composition (marked by the light brown hexagon in Fig. 1), the mass fraction of DAC and the second component (either basalt or quartz sand) was selected so that the final composition of the mixture moved close to the target composition while incorporating as much as possible DAC. In Fig. 1, the mixture compositions (green symbols) lie close to the mixing lines DAC-basalt (SF1 and SF3) and DAC-quartz (SF2), respectively. Batches were designed to be slightly different in composition for the purpose of comparing mechanical and other properties, while remaining closer to the desired target composition. The batches so produced were characterized with a variety of techniques, as illustrated in Table 1.

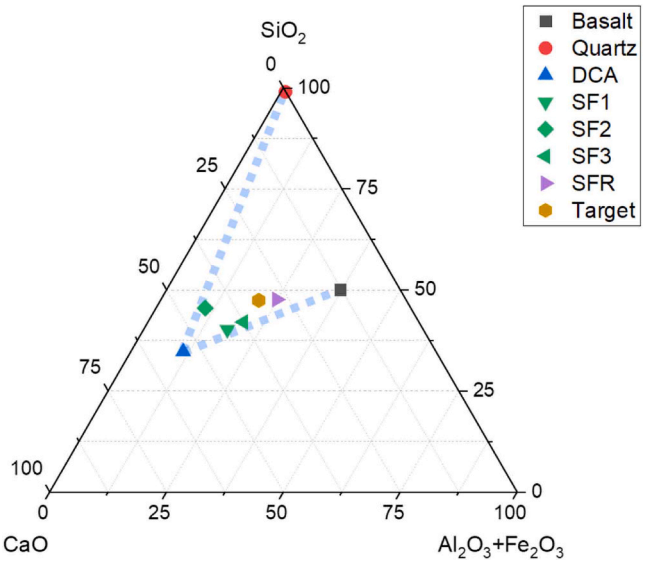

Fig. 1. SiO_2-(Al_2O_3+Fe_2O_3)-CaO ternary diagram reporting the raw material compositions and the composition of the fiberized samples. Pale blue dashed lines represent mixing lines among DAC and the other raw materials.

2.2. Melting and fiberization

Melting and fiberization experiments were conducted at Department for Materials and Metallurgy, Faculty of Natural Sciences of the University of Ljubljana, using an induction melting furnace and a single wheel (ϕ = 250 mm) spinning machine, also known as spinner. The induction melting furnace has a batch capacity of approximately 2 kg of melts and can operate at temperatures of up to 1600 °C. Batches are melted in a graphite crucible heated by a water-cooled furnace winding and can be poured onto the rotating wheel of the spinner by a pivot mechanism (Fig. 2; see Fig. S1 in supplementary materials for photos of the fiberization rig). Fibers form as melt is poured onto the spinning wheel via a channel (typical pouring rate of 0.15 kg/s) with an adjustable transversal position and inclination angle, whereas the rotational speed of the wheel can be controlled by a variable frequency drive (VFD). Forming fibers are then blown away by an axial fan with adjustable speed and collected on a removable containment mesh.

In the present stone wool fabrication experiments, mixture of DAC and basalt or quartz sand were melted and stabilized at ~1500 °C. Once the melt was homogenized, the spinner wheel surface and the V-shaped melt channel were heated by acetylene-oxygen burner to ~200 °C to improve melt adhesion to the wheel and prevent excessive solidification in the channel. The melt was then poured with an impingement angle of $\varphi = 30°$ onto the spinner wheel rotating at 3000 RPM. The velocity of the coaxial air flow above the wheel was approximately 10 m/s.

2.3. Instrumental analyses

X-ray powder diffraction (XRPD) and X-ray fluorescence (XRF) analyses were performed at the Department of Earth and Environmental Sciences (DISAT) of the University of Milano-Bicocca, respectively with a X'Pert-Pro PW3060 diffractometer and an Epsilon 3X energy-dispersive XRF instrument, both by PANalytical. Before the analyses, the sample were powdered manually in an agate mortar.

XRPD analyses were carried out both on fibers and non-fiberized (shot) glass samples. Data were collected at room temperature, at 40 mA and 40 kV in the 5–80° 2θ range. Qualitative phase analysis was carried out with the PANalytical X'Pert High Score software, making use of the ICSD PDF2–2004 database.

For XRF analyses, sample briquettes were prepared by mixing 10 g of powdered material, 5 g of boric acid and few droplets of polyvinyl

Table 1
Brief description of the samples and list of analyses they were subjected to.

Sample	Description	Recipe/Origin	XRF	XRD	SEM	EDS	DSC	SER
DAC	Asbestos-cement slates thermally treated and powdered	Collected by Tecneco SRL; Thermally treated by Petroceramics SRL	√	√	√	√	√	
Basalt	Basalt sand	Commercial aquarium sand	√	√				
Quartz	Quartz sand	From local supplier	√	√				
SF1	Fibers, 1st batch	63.2 % DAC, 36.8 % basalt	√	√	√	√	√	√
SN1	Non-fiberized material			√	√	√		
SF2	Fibers, 2nd batch	77.4 % DAC, 22.6 % quartz	√	√	√	√	√	√
SN2	Non-fiberized material			√	√	√		
SF3	Fibers, 3rd batch	50 % DAC, 50 % basalt	√	√	√	√		√
SN3	Non-fiberized material		√	√	√	√		
SFR	Commercial reference stone wool	Gabbro-diabase with unknown amount of slag and briquettes	√	√	√	√		

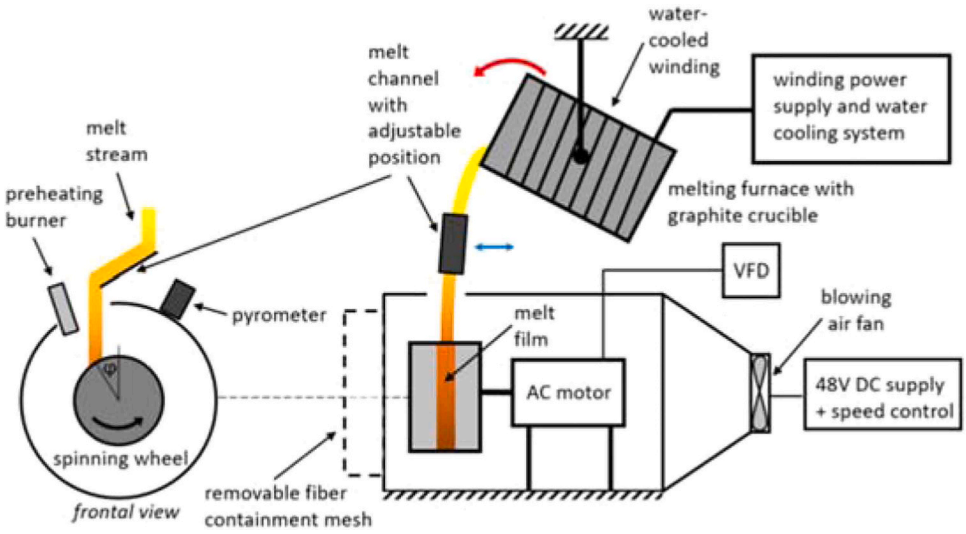

Fig. 2. Melting and fiberization setup for producing fiber samples.

alcohol and pressed at a pressure of 1471 MPa for a minute. The Omnian-standardless method was used for quantitative analyses. Aliquots of the powder were used for volatile components (H_2O plus CO_2) determination through weight loss on ignition (LOI).

Scanning electron microscopy (SEM) observations and energy dispersive spectroscopy (EDS) analyses were performed at the Platform of Microscopy of the University of Milano-Bicocca (PMiB) with a Zeiss Gemini 500 equipped with a Bruker XFlash 6I30 EDS and with a Tescan VEGA TS 5136XM equipped with an EDAX Genesis 4000 EDS. The stone wool fibers were cut and placed on adhesive carbon pads, in turn placed on Al stubs, and carbon coated to enhance their conductivity.

To determine the melting behavior of selected samples, differential scanning calorimetry (DSC) analysis was performed on Netzsch Pegasus DSC 404 F1 instrument from 300 °C up to final temperature of 1500 °C. Two heating/cooling cycles were completed at 10 K/min in inert (N_2) atmosphere. Prior to DSC analysis, raw samples were ignited at 575 °C for 30 min, sieved through 63 μm sieve and demagnetized. Approximately 30 mg of each sample was weighed and pressed into the 85 μL Pt80/Rh20 crucible with lid. The purpose of the first heating-cooling cycle is to eliminate the thermal history of fiber production process, while the second cycle allows for comparison in melting behavior between samples of different composition. From the second heating curve, the characteristic temperatures of *liquidus* (T_L), *solidus* (T_S) and glass transition (T_G) can be obtained. The term *liquidus* marks the temperature above which no crystals can exist in a melt. If melt is homogenized above T_L and then rapidly cooled, amorphous material is formed, which is beneficial for mechanical strength of resulting fibers due to the greater homogeneity of their structure [20]. The *solidus* temperature (T_S) denotes the temperature below which all the melt is fully transformed into crystals upon slow cooling, although it typically remains soft and ductile well below T_S. As the melt continues cooling, it eventually reaches the point of glass transition (T_G), when in a narrow temperature range it is transformed from a rubber-like state to a brittle solid one.

The mechanical properties of the fiber were determined by Sentmanat extensional rheometry (SER) at the Laboratory for experimental mechanics at the University of Ljubljana. Tensile tests were performed on three individual fibers from each mineral wool sample (sample SF1, SF2 and SF3). The fiber under test was attached to the surface of two counter-rotating cylinders and pulled through cylinder rotation until the point of rupture while strain and stress are measured (supplementary Fig. S2). A detailed description of the SER method can be found in Oseli et al. [21].

3. Results and discussion

3.1. EDXRF analysis

All sample compositions were determined on fibers (SF* samples). For batch 3, the bulk composition was determined also for non-fiberized (shot) material (SN3). As can be inferred from Table 2, all samples contain higher fractions of SiO_2 and lower fractions of CaO compared to the DAC and are reasonably close to the target composition. Their compositions plot along the mixing line between DAC and the other raw materials in the SiO_2-(Al_2O_3+Fe_2O_3)-CaO ternary diagram (Fig. 1). The samples with higher proportion of basalt (SF1 and SF3) are also those with the higher content of Al_2O_3, Fe_2O_3, and MgO, since these components are more abundant in basalt than in the other raw materials. In comparison to all the other samples, the sample SF3 is characterized by

Table 2
EDXRF analyses (wt%) of stone wool (S*), basalt, quartz and deactivated asbestos-cement (DAC) raw materials used in the experiments (*b.d.l.* = below detection limit).

	Basalt	Quartz	DAC	SF1	SF2	SF3	SN3	SFR
Na_2O	3.60	*b.d.l.*	0.17	1.02	0.15	1.03	1.02	1.28
MgO	8.55	*b.d.l.*	7.68	8.88	4.92	7.85	7.67	7.66
Al_2O_3	13.73	0.84	3.90	6.99	4.57	8.34	8.46	11.16
SiO_2	40.44	98.64	30.41	34.78	42.30	36.93	37.18	41.89
P_2O_5	0.75	0.01	*b.d.l.*	*b.d.l.*	*b.d.l.*	*b.d.l.*	*b.d.l.*	*b.d.l.*
SO_3	*b.d.l.*	*b.d.l.*	3.11	0.46	0.49	0.30	0.29	0.32
Cl	0.11	*b.d.l.*	*b.d.l.*	*b.d.l.*	*b.d.l.*	0.01	0.02	*b.d.l.*
K_2O	1.17	*b.d.l.*	0.43	0.65	0.49	0.85	0.89	0.59
CaO	10.39	0.10	47.38	36.31	40.92	33.01	32.99	24.29
TiO_2	2.81	0.07	0.23	1.51	0.49	1.09	1.11	1.49
V_2O_5	0.06	*b.d.l.*	*b.d.l.*	0.04	0.01	0.02	0.02	0.07
Cr_2O_3	0.07	0.02	*b.d.l.*	0.07	0.06	0.07	0.05	0.04
MnO	0.24	*b.d.l.*	0.43	0.20	0.14	0.13	0.13	0.28
Fe_2O_3	16.32	0.11	5.93	8.53	5.25	9.61	9.68	10.66
NiO	0.05	*b.d.l.*	*b.d.l.*	0.03	0.02	0.03	0.02	*b.d.l.*
CuO	0.01	*b.d.l.*	*b.d.l.*	0.01	0.01	0.01	0.01	0.02
ZnO	0.02	*b.d.l.*	*b.d.l.*	0.02	0.02	0.02	0.02	0.01
SrO	0.15	*b.d.l.*	*b.d.l.*	0.16	0.09	0.10	0.10	0.08
ZrO_2	0.05	0.06	*b.d.l.*	0.04	0.01	0.02	0.08	0.03
SnO_2	0.03	0.02	*b.d.l.*	*b.d.l.*	0.03	0.01	0.02	0.03
BaO	0.07	*b.d.l.*	*b.d.l.*	0.06	0.02	0.05	0.06	0.03
LOI	1.39	0.14	0.32	0.26	*b.d.l.*	0.51	0.16	0.07

higher Al_2O_3-Fe_2O_3 and lower CaO, with a composition closer to the reference sample (SFR).

The LOI values are very small in all samples, consistently with the high temperatures of the stone wool production process, the thermal inertization of asbestos-cement, and the high crystallization temperature of basalt. The small LOI values detected are probably due to minor rehydration of the samples after their formation. Finally, the bulk composition of the fiber and of the non-fiberized S3 sample are closely comparable, testifying an effective homogenization before the fiberization process.

In order to rationalize, at least qualitatively, the melt behavior of the current multidimensional/multicomponent system, we can refer to the simplified CaO-Al_2O_3-SiO_2-MgO system reported in Fig. 3. It can be observed that the T_L of all fiberized samples is close to 1300 °C, or slightly above the minimum attainable T_L in the given phase diagram. Since it is desired that fibers have a fully amorphous structure, a low T_L is favorable for fiberization since a lower melt working temperatures can be used, saving energy and at the same time preventing crystallization, that cannot occur above T_L.

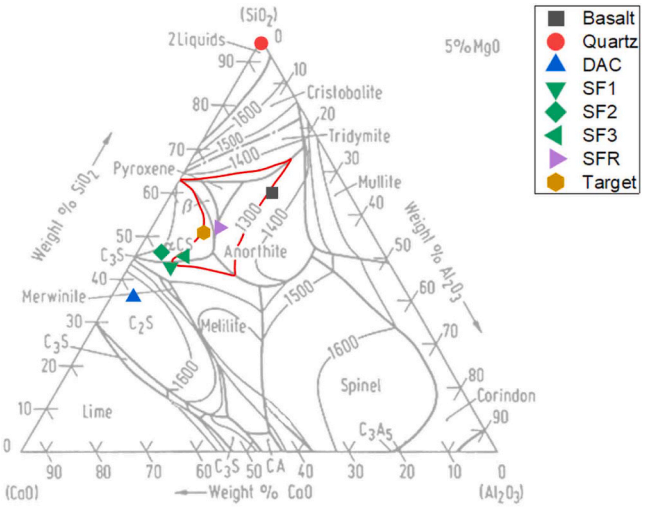

Fig. 3. Raw material and fiberized products compositions on the simplified CaO-Al_2O_3-SiO_2 ternary phase diagram (5 % MgO). The 1300 °C isotherm is highlighted by a red line (after Cavalier and Sandreo-Dendon [22], modified).

3.2. XRPD analysis

XRPD analyses were initially performed on raw materials. The DAC, examined in a previous work [17], contains amorphous material (glass) as major constituent (~40 wt%), then crystalline phases typical of cement, namely åkermanite (~19 %), bredigite (~19 %), merwinite (~18 %) and larnite (~4 %). The quartz sand is practically pure quartz (Fig. 4). The basalt sand comprises as main crystalline phases: augitic pyroxene (~45 %), forsteritic olivine (~15 %), anorthite (15 %), nefeline (~12 %) and sanidine (~12 %); silicatic melt, usually abundant in basalt, was not estimated.

XRPD analyses conducted with extended collection times on all fiberized materials do not reveal peaks indicative of crystalline phases. Only a huge bulge at ~31° 2θ in all sample were observed (Fig. 5). Non-fiberized materials sometimes show small peaks, as for the sample SN1 and SN3. In sample SN1, a single peak related to the (002) reflection of graphite is observed. Graphite probably resulted from the combustion of organic material that accidentally contaminated the batch. In sample SN3, the observed peaks belong to åkermanite ($CaMg_2Si_2O_7$), a high temperature phase forming a solid solution with gehlenite ($Ca_2Al_2SiO_7$), with a melting point between 1388 and 1590 °C [23], which was present in the DAC raw material and that evidently resisted melting.

3.3. SEM-EDS observations

All the observed fiberized samples appear very similar (Fig. 6) and resemble the reference sample (Fig. 7). The diameter of the fibers ranges from few microns to several tens of microns, although the majority has a diameter lower than 10 μm. The surface of the fibers is rounded and smooth and, in general, there is no compositional variation detectable with the backscattered electrons (BSE). EDS analyses reveal Si, Ca, Mg, Al, Fe, Na, in the order, as major cations and minor amounts of K, S, P and Ti (Fig. 6 and Table 3). Occasionally, small particles with higher BSE yield can be observed on the fibers, identified as Fe-Cr particles with EDS spectroscopy (Fig. 7D). These particles are present in all the studied samples and may represent external contaminations by dust or wore parts of the fiber production machinery.

SEM-EDS analyses on single fibers are qualitatively in-line with EDXRF results, but the MgO, SiO_2, Al_2O_3 contents, on one side, and the CaO and Fe_2O_3 contents, on the other side, are systematically over-estimated and underestimated, respectively, in comparison to EDXRF (cf. Table 3 with Table 2). This is probably due to the lower accuracy of

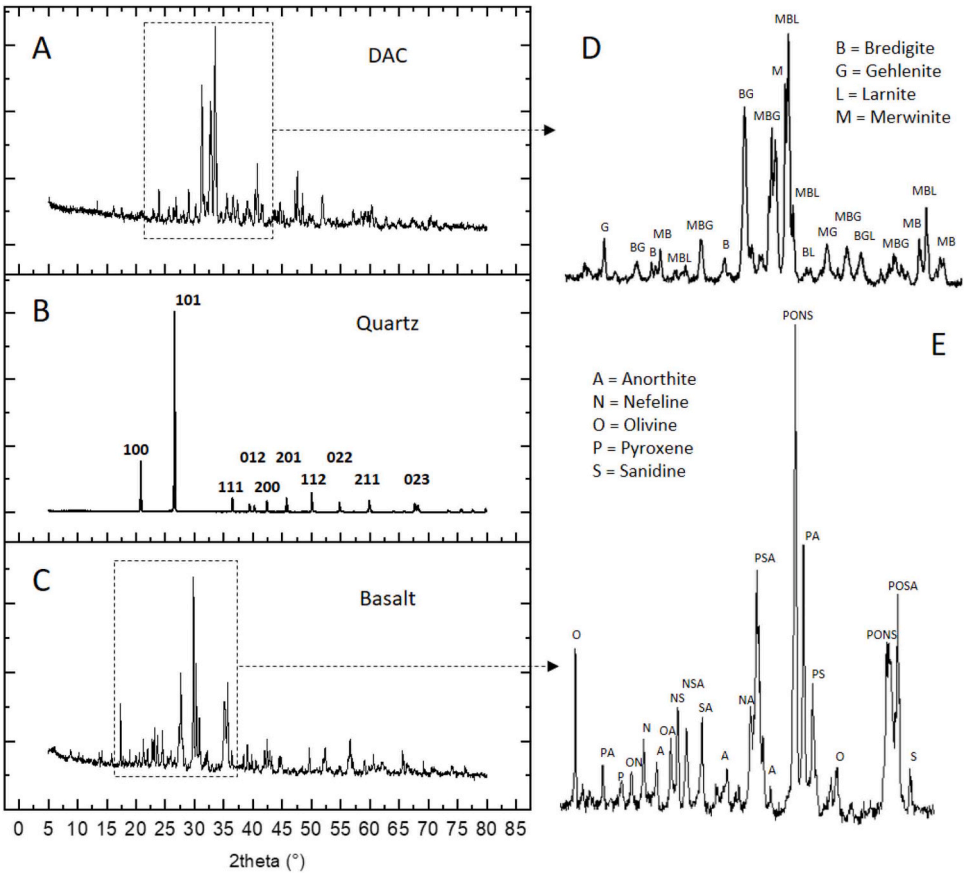

Fig. 4. XRPD patterns of raw materials: (A) DAC; (B) quartz; (C) basalt. The main peaks and the phases that contributed to them are indicated for DAC (D) and basalt (E). For quartz, crystallographic planes contributing to the main diffraction peaks are indicated.

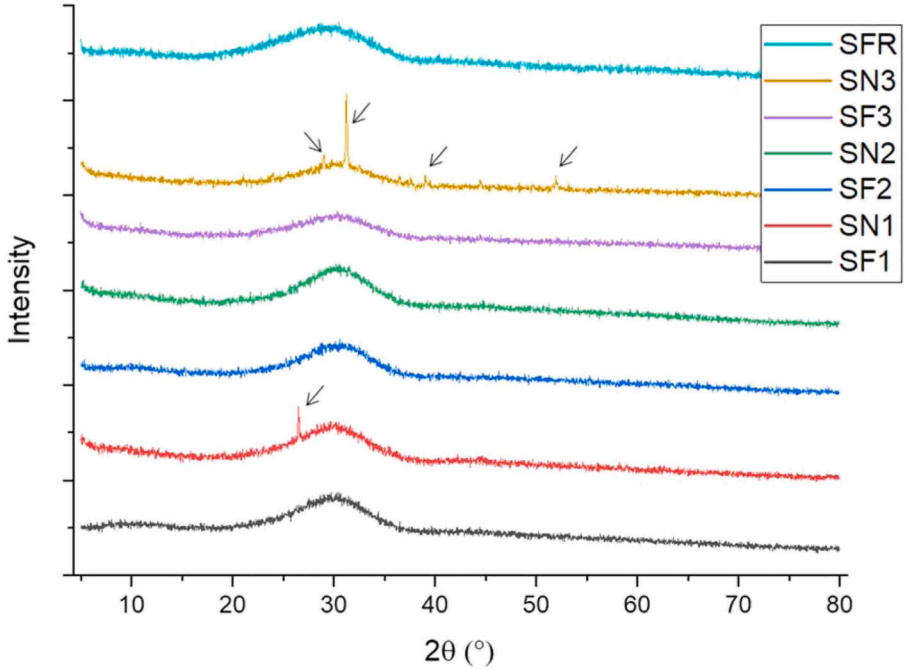

Fig. 5. XRPD patterns of fiberized (SF*) and non-fiberized (SN*) DAC-bearing materials and reference, DAC-free sample (SFR). All batches are completely amorphous. The small peak at ~26.5° in the SN1 and those in the SN3 non-fiberized samples (arrows) belong to the graphite (002) peak and to åkermanite, respectively (see text for explanation).

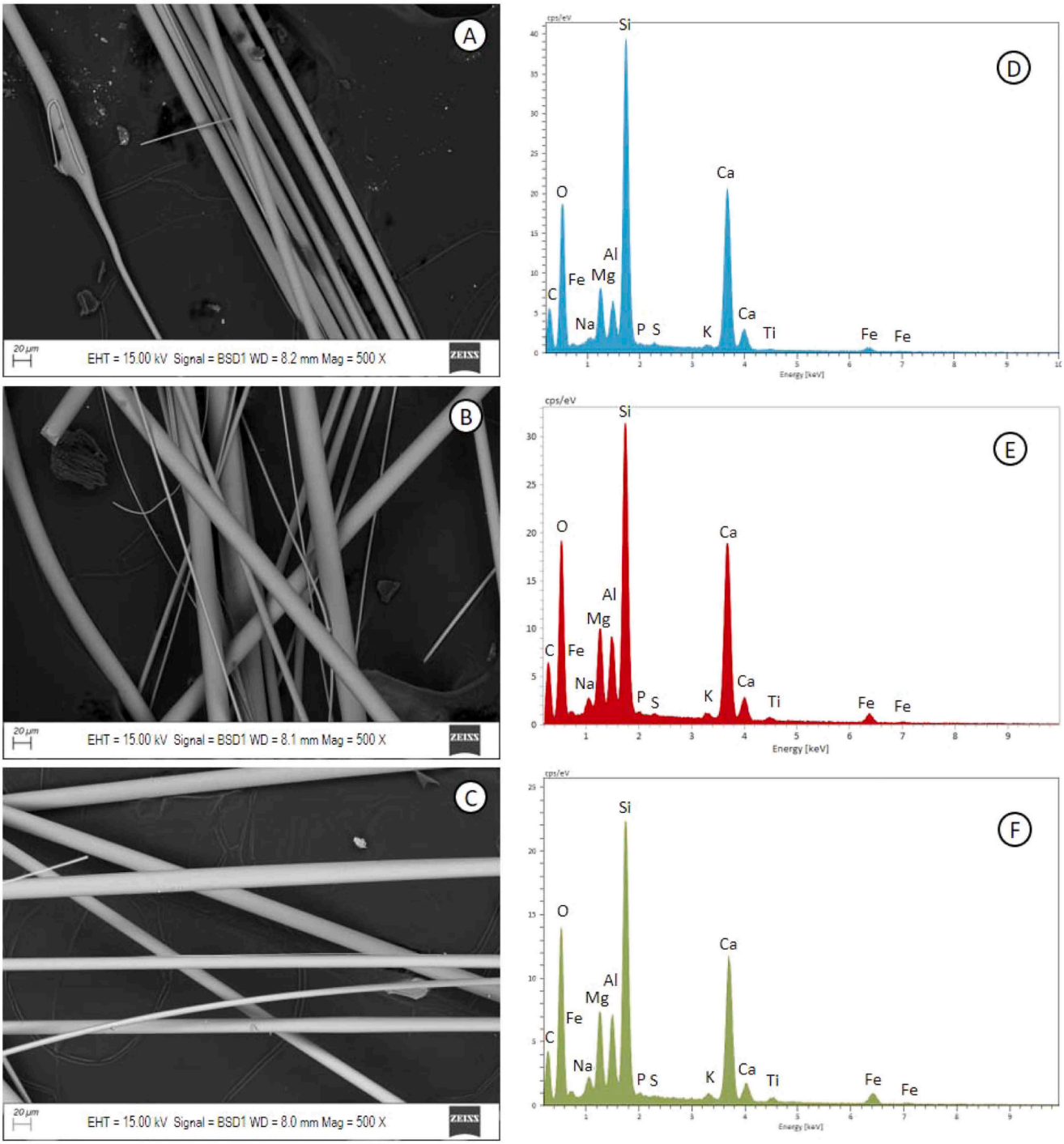

Fig. 6. SEM-BSE images of stone wool sample SF1 (A), SF2 (B), and SF3 (C) and related representative spectra (E to F).

the SEM-EDS analysis in comparison to EDXRF and not to chemical fractionation during fiberization.[1] Indeed, the comparison between fiberized (SF*) and non-fiberized materials (SN*) do not show any significant difference, apart for sample 2, where the non-fiberized material is higher in SiO_2 than the corresponding fibers. In this case, it is very probable that the silica-rich material could not be fiberized because of the raised viscosity, which increases with increasing silica. Representative images of the non-fiberized material and their spectra are reported in the supplementary material (Fig. S3).

Overall, the fiber composition seems rather homogeneous from fiber to fiber, as testified by the lower standard deviations (Table 3), except, again, sample 2, which shows the highest deviations. It seems, therefore, that the DAC-quartz mixture in the ~3:1 proportion used in the experiments could cause problems related to the high viscosity of silica during the homogenization process and, consequently, during fiberization.

3.4. DSC analysis

Characteristic temperatures T_L, T_S and T_G are shown in Fig. 8 along

[1] Accurate SEM-EDS analysis requires a sample prepared as to expose flat, polished, conductive surfaces and a calibration against standard of known composition, which was not the case here.

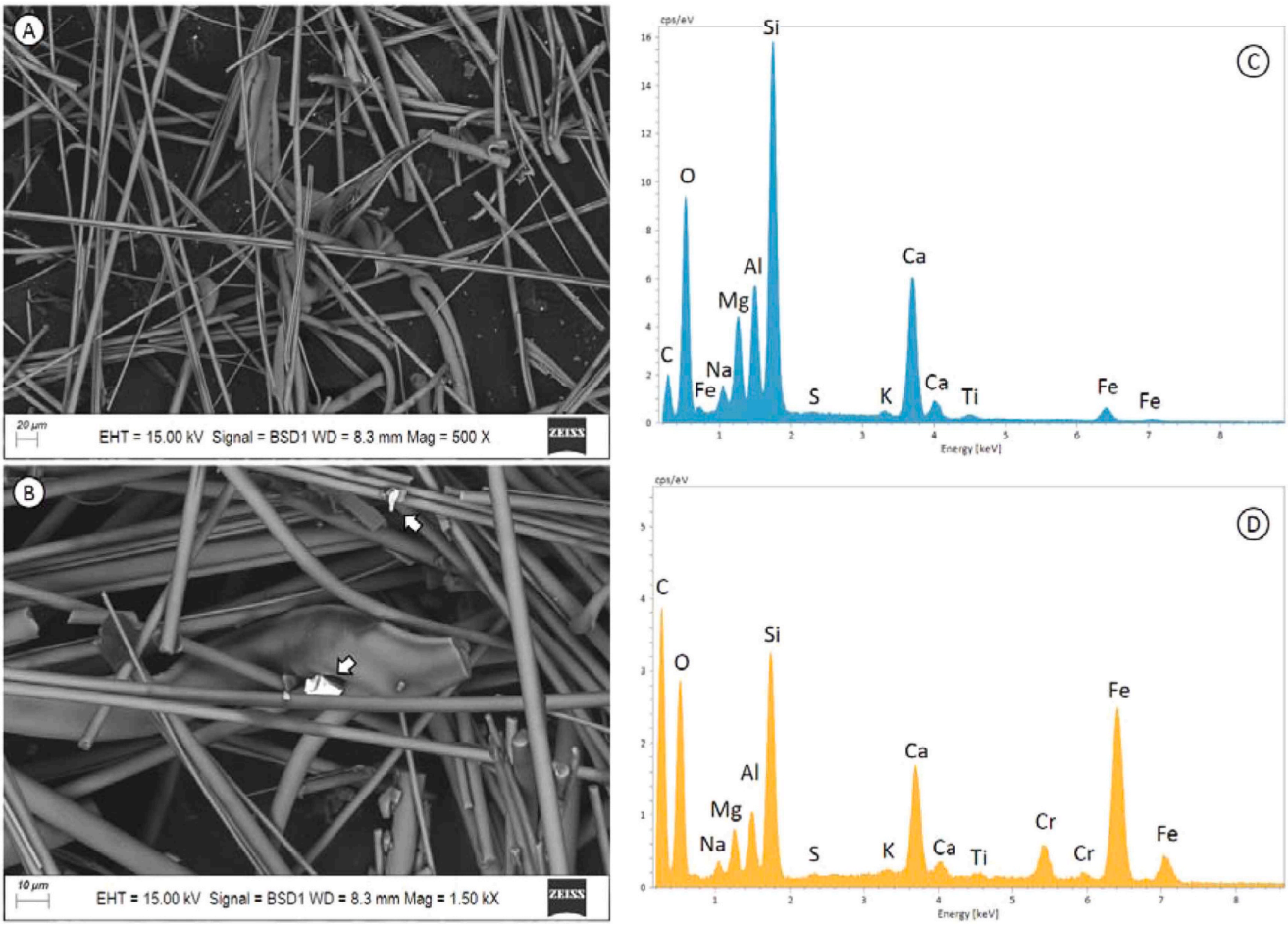

Fig. 7. SEM-BSE images (A and B) and EDS spectra (C and D) of reference sample SFR. Arrows in (B) indicate some dust particles: (C) Representative EDS spectrum of stone wool fibers; (D) EDS spectrum of a Fe-Cr particle. All the other peaks are from the fibers.

Table 3
Average SEM-EDS semi-quantitative analyses (wt%) of stone wool samples and non-fiberized material (number of averaged analyses between brackets).

	SF1		SN1		SF2		SN2		SF3		SN3		SFR	
	Mean (11)	Sigma	Mean (4)	Sigma	Mean (9)	Sigma	Mean (4)	Sigma	Mean (10)	Sigma	Mean (2)	Sigma	Mean (11)	Sigma
Na_2O	2.07	0.23	2.48	0.33	1.38	0.60	1.15	0.24	2.56	0.25	2.69	0.12	1.66	0.67
MgO	9.37	0.33	9.61	0.41	7.81	1.24	7.11	0.49	9.71	0.41	9.92	0.08	7.61	1.03
Al_2O_3	9.11	0.21	9.26	0.14	6.87	1.81	6.07	0.41	9.85	0.37	9.89	0.03	11.96	0.78
SiO_2	39.32	0.79	38.42	0.30	43.89	3.78	47.39	1.00	38.59	0.93	38.54	0.14	42.76	0.96
P_2O_5	0.39	0.15	0.52	0.08	0.31	0.20	0.25	0.08	0.50	0.12	0.54	0.03	0.02	0.05
SO_3	0.39	0.19	0.41	0.14	0.56	0.11	0.32	0.03	0.24	0.08	0.31	0.04	0.44	0.41
K_2O	0.69	0.05	0.68	0.06	0.55	0.13	0.48	0.05	0.57	0.08	0.54	0.04	0.49	0.06
CaO	32.97	0.87	31.74	0.99	34.52	2.39	33.78	1.38	29.36	1.21	29.30	0.22	26.57	2.29
TiO_2	1.12	0.08	1.12	0.06	0.63	0.39	0.33	0.13	1.62	0.07	1.60	0.15	1.39	0.10
Fe_2O_3	4.57	0.21	5.76	0.64	3.50	0.90	3.12	0.72	7.00	0.25	6.67	0.11	7.11	0.53

with heating and cooling curves from the second DSC cycle. It can be observed that sample SF3 has the lowest *liquidus* temperature among the investigated DAC-containing samples, making it the most suitable composition option. Having said that, T_L of SF3 is still 55 K above the T_L of the reference stone wool sample SFR, meaning that the energy required for melting is still considerably higher than in the case of optimized industrial stone wool batches not containing DAC.

Another important consideration is the difference between the *liquidus* and *solidus* temperature (T_L - T_G). To obtain optimal mechanical properties and reduce melting energy, eutectic-like compositions are pursued, meaning that the value of T_L - T_G should be as low as possible. Once again, SF3 stands out with a T_L - T_G = 126 K, which is significantly lower than for SF1 (169 K), but higher than for SFR (60 K). Note that for SF2, T_G could not be determined due to the lack of distinct curve steepening in expected T_S temperature region. Besides these observations, it can also be noted that T_G is very similar for both basalt-containing samples (i.e., SF1 and SF3) and the SFR sample, while the quartz-containing sample SF2 had a somewhat higher T_G.

If fibers produced from DAC are to be competitive to ordinary stone wool fibers in mechanical properties, T_L must be below the temperature at which melt is fiberized to avoid fiber crystallization. In our case, there is no indication that the melt temperature would be too low (i.e., below T_L), but energy consumption for melting can be reduced if composition is optimized towards lower T_L. However, melt viscosity tends to significantly increase close to eutectic compositions due to increased SiO_2 content. Optimizing the chemical composition for minimum melting

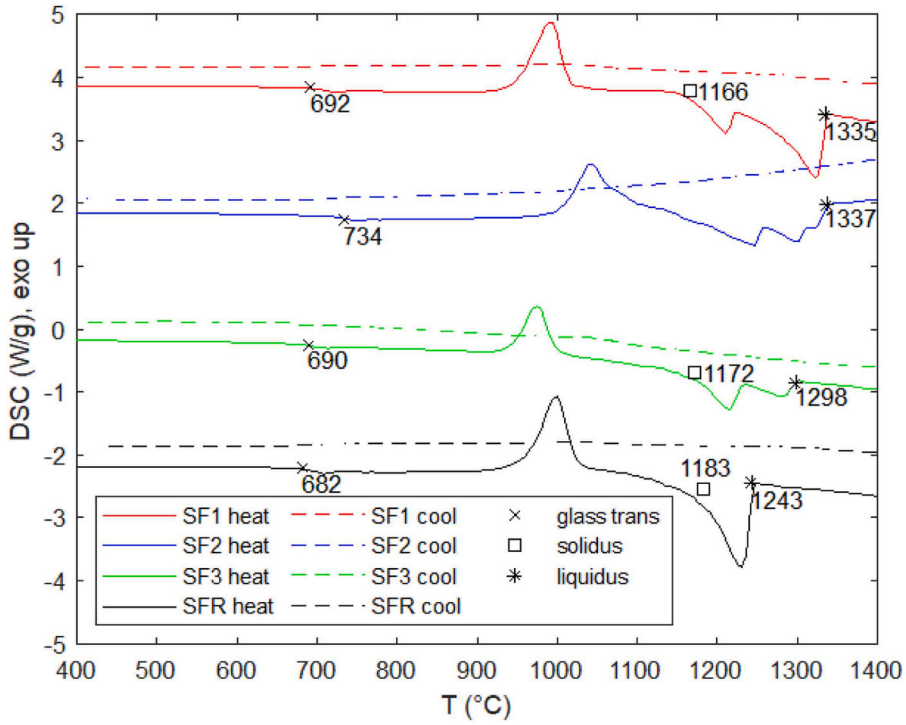

Fig. 8. Temperature dependent DSC curves of mineral wool samples for the second heating and cooling cycle. Also shown are *liquidus*, *solidus* and glass transition temperatures determined from the curves.

energy consumption while retaining adequate fiber biosolubility is a complex task requiring a large number of calorimetric measurements and calculations, and thus beyond the scope of this paper.

Nevertheless, it must be noted that minimizing T_L is not the only possible optimization routine. This approach is only sensible if DAC is added in relatively small percentages to industrial stone wool furnaces. However, if asbestos waste is to be treated separately from industrial stone wool production and fiberized on a small scale, a high degree of DAC utilization (at least 50 %) is preferred to reduce the cost of relatively expensive mineral components such as basalt or quartz sand, as well as excess energy and equipment capacity required to melt these additional components. In this case, the ultimate goal should be to minimize the overall cost per ton of recycling DAC considering both the raw material cost as well as the energy cost while maintaining fiber properties reasonably close to industrial mineral wool.

3.5. Mechanical properties

The result of SER tensile tests are tensile diagrams which allow for calculation of the Young's modulus and tensile strength of fibers. Tensile diagrams for all lab-produced stone wool fiber compositions are shown in Fig. 9, where one tensile curve is displayed for each fiber tested. Note that some scattering can be observed within fiber samples due to fiber impurities and shape irregularities (supplementary Fig. S2). The mean values of measured Young's moduli (E) were as follows: SF1 = 46.3 GPa, SF2 = 69.7 GPa and SF3 = 57.6 GPa.

For comparison, good quality industrial stone wool fibers reach values of E of about 40–60 GPa [21]. As we can see, SF2 has the highest E of all samples analyzed, followed by SF3 and SF1. The Young's moduli of all three DAC-containing samples are comparable to those of good quality industrial stone wool fibers, suggesting similar mechanical stiffness.

Besides Young's modulus, tensile strength is another key parameter that can be determined from tensile diagrams. In tensile measurements

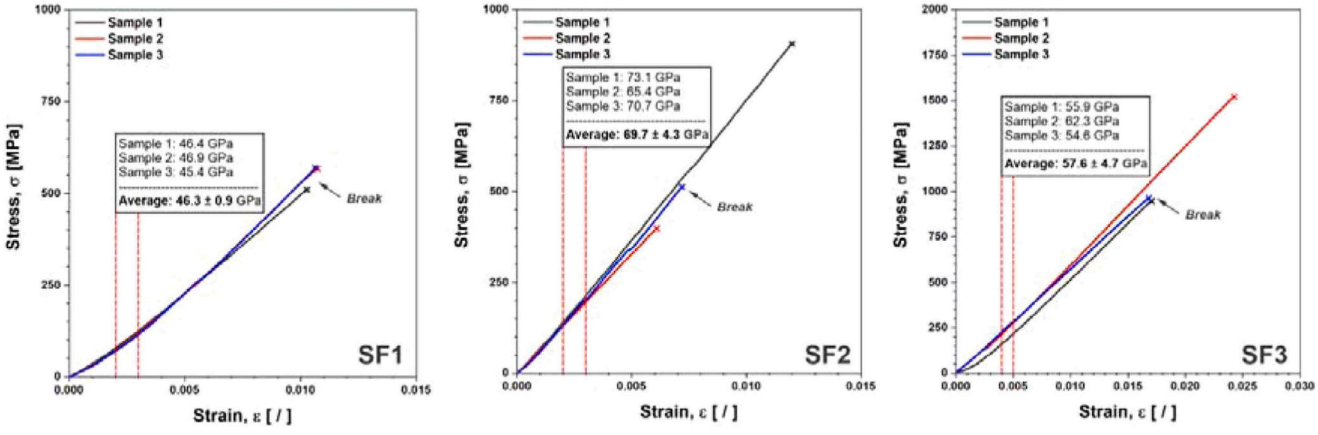

Fig. 9. Tensile diagrams for samples SF1, SF2 and SF3 and related measured Young's moduli (insets).

of fibers from samples SF1, SF2 and SF3, the tensile strength of individual fibers was widely scattered between 400 MPa and 1500 MPa (most fibers ruptured near the lower end of this range), without a clear correlation with chemical composition or *liquidus* temperature. Such a high variability is consistent with findings reported by Lund [24] for regular stone wool fibers. As reported in [21] and [25–29], the mechanical properties of stone wool fibers are profoundly affected by the ceramic content ($SiO_2 + Al_2O_3$). In general, ceramic content from 55 to 70 wt% results in high variation of Young's moduli (from 40 to 90 GPa), and stress at break (from 200 to 3000 MPa), which correlates strongly to the presented results. The range of tensile strength for samples SF1-SF3 is also comparable to industrial stone wool fibers [21,24]. This demonstrates that mineral wool produced from DAC-containing melts can possess mechanical strength just as high as the regular stone wool.

4. Conclusions

In the present work, our main goal was to demonstrate the capability to fiberize deactivated (detoxified) asbestos-cement waste and other raw materials (basalt and quartz sands) into mineral wool of non-toxic composition and with melting temperatures comparable to commercial stone wool, establishing also a methodology for property evaluation of the fibers so produced. So far, based on the experimental results, the most important conclusions are:

1. DAC, basalt and quartz mix well in the furnace, creating homogenous melt that can be poured and fiberized at reasonable temperatures (1500 °C). Target composition range of commercial stone wool can be obtained by a proper mixture of DAC with either basalt or quartz.
2. Samples SF1 and SF3 with 36.8 % and 50 % of basalt produced fibers with composition closer to target than SF2 with 22.6 % of quartz. By further composition optimization and using multiple components instead of just a binary mixture, we estimate that future batches could utilize 70–75 % of DAC, resulting in relatively low cost of added materials and additional energy to melt them.
3. *Liquidus* temperature of mineral wool is similar for compositions 1 and 2 (1335 °C for batch 1 and 1337 °C for batch 2), but notably lower for batch 3 (1298 °C). This means that batches with lower percentage DAC have an advantage over higher percentage DAC batches (note that 100 % of DAC waste cannot be fiberized at temperatures utilized in our experiments). The *liquidus* temperature of sample SF3 is approaching that of typical industrial stone wool, but is still about 50–70 °C higher, meaning that melt pouring temperature also has to be elevated by the same amount relative to industrial wool to prevent fiber crystallization.
4. Mechanical properties: Young's modulus measured by tensile tests was highest for batch 2 (22.6 % quartz – 77.4 % DAC) and exhibits no clear relation with DAC content. Young's modulus and tensile strength of all DAC-containing samples is comparable to good quality commercial stone wool fibers.
5. Further studies should investigate the effect of DAC-containing batch composition on fiber properties in greater detail while also implementing cost optimization of both raw materials and required energy to render the recycling process as economically feasible as possible.

This work is part of a series of studies by our group, both concluded and in progress, concerning the recycling of detoxified asbestos cement in various industrial applications. These include its use as a fluxing agent in ceramic sanitary wares [30], as filler in epoxy resins for flooring applications [31], as additive in mortar for plaster applications [32], and in geopolymers and biopolymers (work in progress). Among these applications, that of stone wool turned out so far as one of the most promising. Notwithstanding, we are aware that stone wool production has its own drawbacks since breathable particles are released in the working environment and may represent a hazard for human health. Moreover, even if the DAC does not longer contain harmful fibers, it may indeed contain a non-negligible aliquot of breathable particles [17]. This prompted us to set up *in vivo* ecotoxicity tests of DAC (work in progress) and to plan *in vitro* biosolubility tests aiming at evaluating the actual toxicity of the rock wool fibers so produced.

Because of the current preliminary stage of the study, we are definitely not suggesting in the present study compositions to be used in industrial-scale stone wool production and, as regard possible application tests, it is suggested to limit them for the moment to materials that minimize the release of breathable particles (e.g. bricks, tiles, sufficiently thick fibers for reinforcement of cement/concrete…).

Along the same lines, another potential advancement of this project could be the direct inertization of ACW during the stone wool production (work in progress), which, if successful, could result in significant energy saving. In such a case, an even more careful handling of ACW prior to thermal treatment is required, which should include an efficient air flow filtration system in the workplace and the adoption of personal protection equipment for the workers.

CRediT authorship contribution statement

Roberto Conconi: Methodology, Investigation, Data curation. **Fabrizio Vergani:** Methodology, Investigation, Data curation. **Giancarlo Capitani:** Writing – original draft, Validation, Supervision, Project administration, Funding acquisition, Conceptualization. **Benjamin Bizjan:** Writing – original draft, Methodology, Investigation, Data curation, Conceptualization. **Alen Oseli:** Methodology, Investigation, Data curation. **Lidija Slemenik Perše:** Methodology, Investigation, Data curation. **David Bombač:** Methodology, Investigation, Data curation. **Primož Mrvar:** Methodology, Investigation, Data curation.

Declaration of Competing Interest

The authors declare that they have no known competing financial interests or personal relationships that could have appeared to influence the work reported in this paper.

Data availability

Data will be made available on request.

Acknowledgements

This paper was supported by the projects: DEAR (Deattivazione Efficiente dell'Amianto e Riutilizzo), funded by the Italian Ministry of the Ecologic Transition (project n. H45I20000130001); A-FIRE (Asbestos Fast Inertization and Recycling), funded by Fondazione Cariplo within the call "Cariplo 2020-Circular Economy for a Sustainable Future" (project n. H45F20000480007); by the Slovenian Research Agency (Research Program P2-0264) and by the Italian Ministry of University and Research (MIUR) through the "Dipartimenti di Eccellenza–2019" grant.

Appendix A. Supporting information

Supplementary data associated with this article can be found in the online version at doi:10.1016/j.conbuildmat.2024.137351.

References

[1] A.F. Gualtieri, Mineral fibre-based building materials and their health hazards. in: Toxicity of Building Materials, Elsevier, 2012, pp. 166–195, https://doi.org/10.1533/9780857096357.166.
[2] H.C.V. Skinner, M. Ross, C. Frondel, Asbestos and other Fibrous Materials: Mineralogy, Crystal Chemistry, and Health Effects, Oxford University Press, New York, 1988.
[3] G.D. Guthrie, B.T. Mossman, Health effects of mineral dust, Reviews in Mineralogy, 28, De Gruyter, Berlin, Boston, 1993. https://doi.org/10.1515/9781501509711.

[4] C.S. Dela Cruz, L.T. Tanoue, R.A. Matthay, Lung cancer: epidemiology, etiology and prevention, Clin. Chest Med. 32 (2011) 605–644, https://doi.org/10.1016/j.ccm.2011.09.001.
[5] M. Carbone, H. Yang, Molecular pathways: targeting mechanisms of asbestos and erionite carcinogenesis in mesothelioma, Clin. Cancer Res. 18 (2012) 598–604, https://doi.org/10.1158/1078-0432.CCR-11-2259.
[6] A. Reid, N.H. De Klerk, C. Magnani, D. Ferrante, G. Berry, A.W. Musk, E. Merler, Mesothelioma risk after 40 years since first exposure to asbestos: a pooled analysis, Thorax 69 (2014) 843–850, https://doi.org/10.1136/thoraxjnl-2013-204161.
[7] D. Marsili, A. Angelini, C. Bruno, M. Corfiati, A. Marinaccio, S. Silvestri, P. Comba, Asbestos ban in Italy: a major milestone, not the final cut, Int. J. Environ. Res. Public. Health 14 (2017) 1379, https://doi.org/10.3390/ijerph14111379.
[8] F. Paglietti, S. Malinconico, B.C. della Staffa, S. Bellagamba, P. De Simone, Classification and management of asbestos-containing waste: European legislation and the Italian experience, Waste Manag. 50 (2016) 130–150, https://doi.org/10.1016/j.wasman.2016.02.014.
[9] M. Corfiati, A. Scarselli, A. Binazzi, D. Di Marzio, M. Verardo, D. Mirabelli, V. Gennaro, C. Mensi, G. Schallemberg, E. Merler, C. Negro, A. Romanelli, E. Chellini, S. Silvestri, M. Cocchioni, C. Pascucci, F. Stracci, E. Romeo, L. Trafficante, I. Angelillo, S. Menegozzo, M. Musti, D. Cavone, G. Cauzillo, F. Tallarigo, R. Tumino, M. Melis, S. Iavicoli, A. Marinaccio, Epidemiological patterns of asbestos exposure and spatial clusters of incident cases of malignant mesothelioma from the Italian national registry, BMC Cancer 15 (2015) 286, https://doi.org/10.1186/s12885-015-1301-2.
[10] L. Vogel, Special report on Asbestos in the world, Hesa Newsl. 27 (2005) 7–21.
[11] J.H. Brand, K.L. Spencer, F.T. O'shea, J.E. Lindsay, Potential pollution risks of historic landfills on low-lying coasts and estuaries, WIREs Water 5 (2018) 1–12, https://doi.org/10.1002/wat2.1264.
[12] R.P. Beaven, A.M. Stringfellow, R.J. Nicholls, I.D. Haigh, A.S. Kebede, J. Watts, Future challenges of coastal landfills exacerbated by sea level rise, Waste Manag. 105 (2020) 92–101, https://doi.org/10.1016/j.wasman.2020.01.027.
[13] L.P. Thives, E. Ghisi, J.J.T. Júnior, A.S. Vieira, Is asbestos still a problem in the world? A current review, J. Environ. Manag. 319 (2022) 115716, https://doi.org/10.1016/j.jenvman.2022.115716.
[14] G. Frangioudakis Khatib, I. Hollins, J. Ross, Managing asbestos waste using technological alternatives to approved deep burial landfill methods: an Australian perspective, Sustainability 15 (2023) 4066, https://doi.org/10.3390/su15054066.
[15] D. Spasiano, F. Pirozzi, Treatments of asbestos containing wastes, J. Environ. Manag. 204 (2017) 82–91, https://doi.org/10.1016/j.jenvman.2017.08.038.
[16] V. Paolini, L. Tomassetti, M. Segreto, D. Borin, F. Liotta, M. Torre, F. Petracchini, Asbestos treatment technologies, J. Mater. Cycles Waste Manag. 21 (2019) 205–226, https://doi.org/10.1007/s10163-018-0793-7.
[17] F. Vergani, L. Galimberti, N.M. Marian, G. Giorgetti, C. Viti, G.C. Capitani, Thermal decomposition of cement–asbestos at 1100 °C: how much "safe" is "safe"? J. Mater. Cycles Waste Manag. 24 (2022) 297–310, https://doi.org/10.1007/s10163-021-01320-6.
[18] D. Bombač, M. Lamut, P. Mrvar, B. Širok, B. Bizjan, Physical properties of mineral fibers depending on the mineralogical composition, Materials 14 (2021) 6108, https://doi.org/10.3390/ma14206108.
[19] Z.S. Yap, N.H.A. Khalid, Z. Haron, A. Mohamed, M.M. Tahir, S. Hasyim, A. Saggaff, Waste mineral wool and its opportunities—a review, Materials 14 (2021) 5777, https://doi.org/10.3390/ma14195777.
[20] Y. Yue, Z. Qiuju, Fiber spinnability of glass melts, Int. J. Appl. Glass Sci. 8 (2017) 1–11, https://doi.org/10.1111/ijag.12254.
[21] A. Oseli, B. Bizjan, E. Krol, B. Širok, L. Slemenik Perše, Tensile properties of mineral fibers determined with Sentmanat extensional rheometer, Constr. Build. Mater. 253 (2000) 119215, https://doi.org/10.1016/j.conbuildmat.2020.119215.
[22] G. Cavalier, M. Sandreo-Dendon, Rev Métallurg, in: M.B.H. Verlag Stahleisen, Schlackenatlas, Düsseldorf, 1981, 1143-1157.
[23] R.A. Mendybaev, F.M. Richter, A.M. Davis, Reevaluation of the akermanite-gehlenite binary system, in: proceedings of the Thirty Seventh Lunar and Planetary Science Conf. Abstr., No. 2268, Woodlands (TX) (No. 2268) (2006) (Woodlands (TX)).
[24] M. Lund, Tensile strength of Glass Fibres (Ph.D.), Aalborg University, (2010), Unpublished Results.
[25] T. Deak, T. Czygany, Chemical composition and mechanical properties of basalt and glass fibers: a comparison, Text. Res. J. 79 (7) (2009) 645–651, https://doi.org/10.1177/0040517508095597.
[26] K.C. Mills, L. Yuan, Z. Li, G.H. Zhang, K.C. Chou, A review of the factor affecting the thermophysical properties of silicate slags, High. Temp. Mater. Process. 31 (4) (2012) 301–321, https://doi.org/10.1515/htmp-2012-0097.
[27] J. Liao, Y. Zhang, S. Sridhar, X. Wang, Z. Zhang, Effect of $Al2O_3/SiO_2$ ratio on the viscosity and structure of slags, ISIJ Int. 52 (5) (2012) 753–758, https://doi.org/10.2355/isijinternational.52.753.
[28] Y.H. Kim, J.M. Park, S.W. Yoon, J.W. Lee, M.K. Jong, R.I. Murakami, The effect of moisture absorption and gel-coating process on the mechanical properties of the basalt fiber reinforced composites, Int. J. Ocean Syst. Eng. 1 (3) (2011) 148–154, https://doi.org/10.5574/IJOSE.2011.1.3.148.
[29] C. Ralph, P. Lemoine, J. Summerscales, E. Archer, A. McIlhagger, Relationship among the chemical, mechanical and geometrical properties of basalt fibers, Text. Res. J. (2018) 1–11, https://doi.org/10.1177/0040517518805376.
[30] A. Bernasconi, L. Pellegrino, F. Vergani, F. Campanale, N.M. Marian, L. Galimberti, M. Perotti, C. Viti, G. Capitani, Recycling detoxified cement asbestos slates in the production of ceramic sanitary wares, Ceram. Int. 49 (2023) 1836–1845, https://doi.org/10.1016/j.ceramint.2022.09.147.
[31] F. Campanale, F. Vergani, N.M. Marian, C. Viti, A. Bianchi, S. Ferrario, M. Mauri, G. Capitani, Epoxy resins for flooring applications, an optimal host for recycling deactivated cement asbestos, Polymers 15 (2023) 1410, https://doi.org/10.3390/polym15061410.
[32] G. Capitani, M. Dalpiaz, F. Vergani, F. Campanale, R. Conconi, S. Odorizzi, Recycling thermally deactivated asbestos cement in mortar: a possible route towards a rapid conclusion of the "asbestos problem, J. Environ. Manag. 355 (2024) 120507, https://doi.org/10.1016/j.jenvman.2024.120507.